JOURNAL OF AIRCRAFT
Vol. 36, No. 4, July–August 1999

Boomerang Flight Mechanics: Unsteady Effects on Motion Characteristics

Manuela Battipede*
Politecnico di Torino, 10129 Torino, Italy

A simulation program is described for predicting boomerang behavior as a function of its geometric characteristics, the throw parameters, and the environmental conditions. It takes into account any nonstationary states that correspond to some motion steps, such as the throw, the transition from helicopter mode to autogyro mode, and the landing. These phases have a significant effect on the characteristics of the trajectory. The boomerang is adopted as a lifting rotor and the nonlinear Pitt–Peters dynamic inflow model is applied, even at very high values of the advance ratio. The mathematical model is strongly nonlinear and therefore highly dependent on initial conditions. The influence of varied environmental conditions as well as of different geometric and throw parameters is highlighted through graphical comparison of the geographic trajectories. Each qualitative trend has been tried and tested; this may be taken as initial confirmation of the reliability of the numerical code. Finally, a complete flight is described and analyzed from all angles, and the need to use an unsteady model is demonstrated through a time–topographical analysis of the advancing blade angles of attack.

Nomenclature

C_T, C_L, C_M	= thrust, rolling moment, pitching moment in wind axis
C_T, C_1, C_2	= thrust, rolling moment, pitching moment in body axis
Eg_{tot}	= total energy
J	= inertia matrix
k_e	= spring elastic constant
$[L]$	= inflow gain matrix
$[M]$	= matrix of apparent mass
MTA	= maximum time aloft
m	= mass or element of $[M]$
$\boldsymbol{p}$	= coordinates of the system, center of gravity
$\boldsymbol{q}$	= quaternions
R	= boomerang radius
r	= radial location or yaw rate
TA	= time aloft
U_P	= parallel component of local velocity
U_T	= tangential component of local velocity
V	= mass-flow parameter due to cyclic disturbances
$[V]$	= matrix of mass-flow parameters
V_{eff}	= effective local velocity
V_T	= total resultant flow through the disk
$\boldsymbol{v}_B^T = (u, v, w)$	= linear velocity vector of the system, center of gravity
$\boldsymbol{v}_i^T = (v_0, v_{c_i}, v_{s_i})$	= vector of induced velocities
$\boldsymbol{X}$	= state vector
α	= local angle of attack or wake angle
$\lambda^T = (\lambda_0, \lambda_c, \lambda_s)$	= nondimensional vector of induced velocities
ρ	= density
$\Phi^T = (\varphi, \theta, \psi)$	= Euler's angles
ψ	= azimuth angle or yaw Euler's angle
$\omega_B^T = (p, q, r)$	= vector of rotational velocity

Subscripts

A	= apparent
aero	= aerodynamic
B	= body reference frame
into	= into the wind
NED	= North-East-Down reference frame
nl	= nonlinear
nw	= no wind
off	= off the wind
S	= sphere
st	= steady
unst	= unsteady
0.7	= 70% of Cl
1	= 100% of Cl
70	= $\phi_p = 70$ deg
80	= $\phi_p = 80$ deg
83	= $\phi_p = 83$ deg
370	= $k_e = 370.5$ Nm
494	= $k_e = 494$ Nm

Introduction

THE classical two-bladed shape is only one of the boomerang configurations, but it is surely the most widespread and oldest model in use. Originally, the boomerang was made of a flat wooden stick, the arm of which could be shaped into varied lengths. Nowadays, interest stirred up by international competitions has led to the introduction of strongly competitive boomerangs made of high-tech materials. The shapes can be the symmetric or asymmetric two-bladed one or the symmetric multibladed one; it also can represent letters of the alphabet, such as X, V, T, H, and Y.

Depending on its shape, material, and dimensions, however, there is a suitable boomerang for each competitive event, considering that one may have a greater natural bent to accomplish a particular trajectory. Indubitably, the thrower's arm and the wind conditions also play important roles. The most traditional and suggestive trajectory is the figure eight, but sometimes the second circle of the eight is so little that it becomes undetectable and the trajectory appears to adopt a circular shape. In other cases the boomerang reaches the highest point within a series of diminishing circles that mark out a spiral, finally landing vertically on the ground.

Whatever the characteristics of the boomerang are, the physical phenomena that are at the basis of its behavior are the same. In the next section, they are described qualitatively, with close attention given to the classical two-bladed version. As explained thereafter, the boomerang is a combination of a gyroscope system and a highly autorotative rotor. A brief survey of the rotor modeling basis introduces the section that describes the calculation process.

Presented as Paper 97-3589 at the AIAA Atmospheric Flight Mechanics Conference, Boston, MA, 10–12, August 1997; received 17 August 1997; revision received 18 January 1999; accepted for publication 21 February 1999.

*Ph.D. Student, Dipartimento di Ingegneria Aeronautica e Spaziale, C.so Duca degli Abruzzi 24; gili@polito.it. Student Member AIAA.

This latter is divided into two phases: first, the constrained motion, which simulates the throw moment; second, the free motion, which represents the flight phase. This latter includes the moment straight after the throw, the climb, the descent, and the landing. The length of these phases is comparable to the characteristic time of the aerodynamic phenomena, and so, great emphasis is put on the unsteady effects on the boomerang modelization.

In the fourth section a complete flight is described by analyzing the trends of the motion variables obtained as a result of the simulation program for a test boomerang. The fifth section presents, as a partial verification of the numerical code, an analysis of the influence of the different aerodynamic and atmospheric variables as well as that of the throw parameters. The last section closely analyzes the results of the numerical simulation: The topographical time-history reconstruction of the angles of attack of the advancing blade further confirms the theory presented in the second section.

The current scientific literature on this subject is very poor; nevertheless, some interesting articles can be found. Among the others, Ref. 1 is a popular paper but it is worth being quoted because it gives testimony on a scientific approach to making very competitive boomerangs: It explains the use of the Buckingham–pi analysis in designing miniaturized boomerangs, which are easier to throw and catch. Hess[2] addresses the problem of the trajectory determination. He proposes a simulator that makes use of a rather dubious model; in fact, he likens the arms of the boomerang to a wing that moves and rotates, but he does not consider, in any way, the effects of the wake. Actually, he finds some inconsistencies and blames them on a poor aerodynamic model; he distinguishes the ideal behavior from the calculated one, highlighting the hypothesis of the presence of numerical perturbations. Furthermore, he tries to refine the model through qualitative comparison with the trajectories that he takes from a real model (this is the only paper that reports some experimental information). In a descriptive book, noteworthy for its completeness, Pignone[3] describes in detail the art of manually crafting and tuning a boomerang, as well as giving some precious advice to improve throwing technique.

Qualitative Interpretation

This section introduces the phenomena involved in boomerang flight, from a qualitative point of view. This description supplies a more complete study on the subject and justifies the hypotheses that surround the model.

A boomerang is nothing more than an eccentric-hub rotor, consisting of high-efficiency airfoils fitted at a nearly null angle. In this statement two different concepts arise: They concern the main characteristics that a good boomerang should have to perform a typical flight.

1) *Rotor autorotative ability:* Autorotation is the well-known regime in which the rotor is moved by aerodynamic forces, through a nonstop extravasation of energy from potential to kinetic. In the case of a helicopter, autorotation is the phase that follows an engine failure: No longer sustained by the engine power, the helicopter starts to descend, acquiring a positive w velocity component (see Fig. 1). The resulting local angles of attack would lead to stall if the pilot did not complete the maneuver to enter into autorotation, which involves a rapid reduction of the collective pitch, that is, of the airfoil incidence. The boomerang has no controls, meaning that the only way to supply it with the autorotative ability is to directly shape it with very low angles of incidence. A suitable airfoil is the flat-convex one, which generally has a high efficiency value and, therefore, features a high value of lift at null angle of attack. Obviously, the autorotation will be involved only during the descent phase of the trajectory, acting as the motive power against the airfoil drag in the rotational motion. Note that, during the ascent phase, the rotational velocity component r increases because of the angular momentum that is conveyed to the boomerang in the throw moment; on the contrary, increasing or constant r value during the descent phase (see the r trend in Fig. 2) can be attributed to the establishment of an autorotational state. As a rule, this feature is common to a good boomerang, that is, a boomerang that can accomplish long flights or precise returns. [One of the targets of the international competitions is called

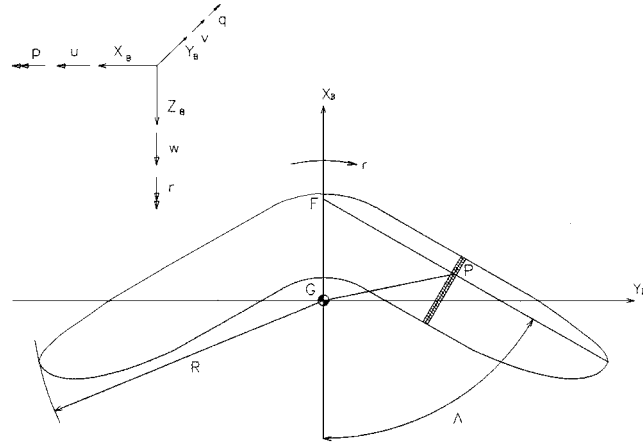

Fig. 1 Reference frames.

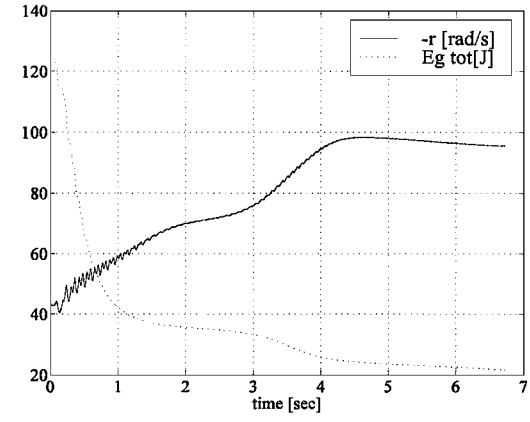

Fig. 2 Component of rotational speed along the z_B axis. Note that it is negative (this is consistent with the thrower being right handed). The total energy also is traced; it has been evaluated by adding kinetic and potential energy contributions (TA = 6.725 s).

Maximum Time Aloft (MTA): It consists of making the boomerang stay up for the longest time. Reference 1 quotes a Swedish inventor who designed an MTA composite boomerang, made of Kevlar®, styrofoam beads, and epoxies, which stayed aloft for 17 min.]

A really good boomerang also is able to perform the last tract of the trajectory in vertical autorotation. Naturally, it may happen that even a strongly autorotative boomerang will perform the classical circular trajectories, never entering in the autorotational state because of a bad throw.

2) *Gyroscopic characteristics:* The two-bladed boomerang is not quite a gyroscope, which is a rotating body with a round inertial ellipsoid, but it can always be defined as a system characterized by high gyroscopic stability. Its swept angle has the sole aim of making the J_{yy} inertial moment of the same order of magnitude of J_{xx}, as shown in Fig. 3. The boomerang gyroscopic qualities depend directly on the extent to which this condition is fulfilled. This fact explains the reason why the inertia matrix is a very important input parameter, requiring careful evaluation. An easy and efficient method to do this is by using a three-dimensional computer-aided design (CAD), which must be fitted with a volume calculation module. By adopting the geometric parameters and the airfoil shape, it is possible to build a mock-up, to which one assigns a material, that is, the density, and therefore the weight. The inertia matrix strictly depends on the swept angle, as stated earlier, so that the design phase includes a sequence of attempts accomplished by acting on different parameters, such as the eccentricity (thus the swept angle), the aspect ratio, the tapering, or the dihedral angle. This problem is avoidable with other kinds of boomerangs: Three-bladed or X- or cross-shaped configurations, for example, have a polar symmetry and consequently are more similar to a real gyroscope and therefore more stable in flight.

Table 1 Geometric and inertial parameters

Parameter	Value
R	0.3 m
Chord	0.05 m (constant)
Swept angle	56.2 deg
Dihedral angle	0 deg
$\overline{FG}$	0.0887 m
Mass	0.1308 kg
J_{xx}	$2.25339e^{-3}$ kg · m^2
J_{yy}	$3.44756e^{-4}$ kg · m^2
J_{zz}	$2.59743e^{-3}$ kg · m^2
J_{xy}	$4.1587e^{-5}$ kg · m^2
J_{xz}	$-3.5184e^{-6}$ kg · m^2
J_{yz}	$-6.255e^{-8}$ kg · m^2

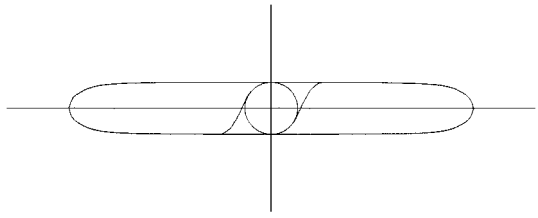

Unstable configuration

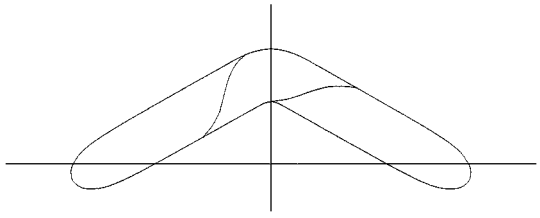

Gyroscopic stability

Fig. 3 Gyroscopic characteristics of two-bladed boomerang.

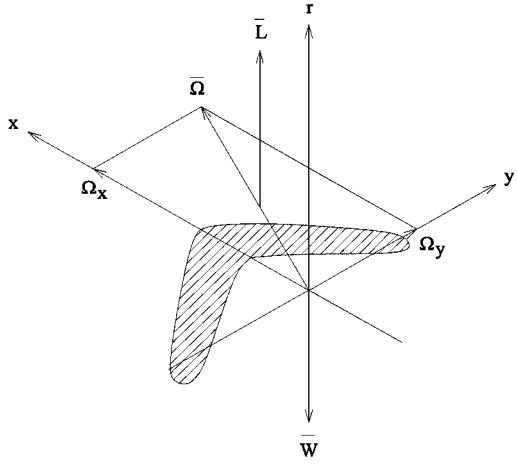

Fig. 4 Precessing motion of the boomerang.

Summing up, in Fig. 4, the fundamental notions of the precessing motion of the boomerang are represented. On average, the application point of the resulting force is supposed to be in front of the advancing blade, whereas the weight is applied in the center of gravity. These two forces produce a moment that, combined with the total rotational velocity, creates a precessional moment that makes the nose of the boomerang go up (this explains the characteristic bending of the trajectory) and the outer blade go down [this motion flattens the boomerang, i.e., the *XY* body plane tends to become parallel to the *XY* North-East-Down (NED) plane].

The results presented here refer to a mock-up created by using a three-dimensional CAD. A medium-sized boomerang was chosen, and a material of unitary density was selected (it might be of seasoned or pressed wood); the geometric and inertial parameters are summarized in Table 1.

Basis of Rotor Modeling

The most interesting aspect of this simulation problem is the calculation of the aerodynamic actions. We know that the aerodynamic behavior of the boomerang is similar to that of a two-bladed rotor made of high-efficiency airfoils fitted at a nearly null angle. During the first part of its trajectory, this rotor works in helicopter mode, that is, it produces the lift required to support the body by accelerating the air mass that passes through the rotor disk in a direction opposite to the lift direction. The rotor is said to be active. If the boomerang is well designed, the second part of the trajectory (return) takes place with the rotor in self-rotation mode: Once the rotation kinetic energy generated by the thrower has run out, the boomerang transforms its potential energy into rotation kinetic energy produced by the aerodynamic forces, which, during this phase, are the driving ones; in this case the rotor is said to be passive. In self-rotation mode, the direction of the resultant velocity is inverted, that is, a transition takes place between the two phases. Apart from this macroscopic aspect, another consideration must be made: boomerang flight is a phenomenon limited in time; that is, a complete time history can be performed in a few seconds, during which motion variables undergo very strong variations. This is to say that a frequency does exist, associated with motion, that obviously will be compared with the natural time taken in the evolution of the physical phenomenon: the higher is the motion frequency, the less time the field has to develop itself, to reach the new operating conditions, and the stronger are the nonstationary effects. Thus, to perform a good simulation, it is necessary to use a sensitive (dynamic) model.

Rotor theory has many examples of modelization attempts, but every method has the same basic idea: to concentrate the problem on the determination of the distribution of the induced velocities; in other words, the determination of the induced velocities is at the heart of the rotor aerodynamics. According to the dynamic inflow theory, inflow is treated globally, as a large mass of air accelerating through the rotor disk. It can be expressed by a function of the radial and azimuthal position, as follows in the first-harmonic relation:

$$v_i = v_0 + v_{i_c}(r/R)\cos\psi + v_{i_s}(r/R)\sin\psi \tag{1}$$

This method was initiated by Curtiss and Shupe[4] in 1971. They laid the foundations for widespread research, inheriting Sissingh's quasisteady formulation,[5] which did not take into account the radial variation of the inflow, the time lag, and the flow perturbations in pitch and roll moments. Since the 1980s, dynamic inflow has been one of the most investigated areas of research.[6,7] It seems to have given some satisfaction: The Pitt–Peters model seems to be quite reliable, complete, and easy to use, even if further work must be done to give it a numerical (experimental) substantiation, beyond that of the methodological one. It is described briefly in the next section, and a justification is given about why it is opportune to apply it to a particular geometry such as that of the two-bladed boomerang. According to the Pitt–Peters model, either the coefficient v_0 or the coefficients of the harmonic terms v_{i_s} and v_{i_c} are functions of the time variable as well as of the aerodynamic loads, and this dependency is expressed by differential equations, to integrate in time. This allows one to follow the evolution of the aerodynamic loads, which are strongly nonstationary. The concept to be underlined is that dynamic inflow is intrinsically a closed-loop problem, as shown in Fig. 5 for the generic case of a controlled machine (helicopter), but the Pitt–Peters model treats it as an open-loop problem, reducing calculation time without loss of generality.

Calculation Process

Each phase of boomerang flight has been simulated: First, we discuss the throwing phase, which represents the constrained-motion phase. Although it is not that interesting from an aeronautical point of view, some discussion is necessary. Imagine a thrower-machine, fitted with a mechanical arm, lying on a plane that is orientable with respect to the NED frame. In correspondence to one tip of the arm, there is the hooking/unhooking boomerang mechanism; on the other side the arm is bound to the plane by a cylindrical torsional spring. It is possible to set the starting and ending points of

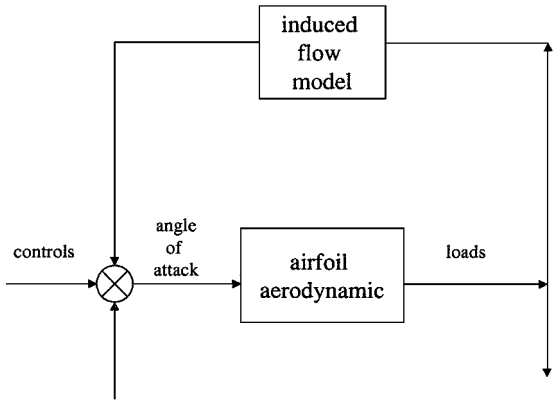

Fig. 5 Dynamic inflow as a closed-loop problem.

the arm's run and calculate the elastic moment to which the arm is subjected. The motion of the arm is planar and is described by three second-order scalar equations, which are integrated instant by instant up to the moment when unhooking takes place. The virtual (simulated) thrower-machine is used for calculating the state vector, and its derivative, in the first instant of the free-motion phase (which coincides with the last instant of the constrained-motion phase). (The idea of the thrower-machine was born from the need to find a way to compare the simulated trajectories with those of a numerical-control model, fitted ad hoc with the very same airfoils used in the test-case model. Employing the thrower-machine solves the problem of imposing the correct initial conditions.)

During the constrained phase, the aerodynamic forces and moments have been neglected. This is not a rough approximation and we can prove it if we compare the inertial end elastic forces with some hypothetical values that the aerodynamic forces would have if they were evaluated in steady condition. Furthermore, this phase wears out in a few split seconds, so that accelerations acquire an impulsive characteristic; aerodynamic forces do not have enough time to develop and reach a value that is even half of the steady one (see Ref. 8 for the case of the impulsive start of the plate). The flight initial state vector is then the result of the balance among inertial, elastic, and gravitational actions. To have good flight performance, extensive power must be put into the boomerang: It literally is hurled by the thrower and undergoes great tangential and centrifugal accelerations, the actions of which influence the whole trajectory, as is pointed out later in the analysis of the results. (Here, trajectory has its wider meaning: It is the locus of points described by the state vector tip, instant by instant, in the phases' space.)

As soon as the free-motion phase starts, the aerodynamic actions and their variations in time begin to play an important role. To perform the simulation, the nonlinear version of the Pitt–Peters dynamic inflow model is used. It consists of a first-order differential vectorial nondimensional equation to be added to the state equations of the rigid body,

$$\begin{bmatrix}\dot\lambda_0\\ \dot\lambda_s\\ \dot\lambda_c\end{bmatrix} = -[M]^{-1}[V][L]^{-1}\begin{bmatrix}\lambda_0\\ \lambda_s\\ \lambda_c\end{bmatrix} + [M]^{-1}\begin{bmatrix}C_T\\ C_1\\ -C_2\end{bmatrix}_{\text{aero}} \tag{2}$$

in which

$$[\lambda] = \begin{bmatrix}\lambda_0\\ \lambda_s\\ \lambda_c\end{bmatrix} \tag{3}$$

is the nondimensional induced velocity vector in body axis. (The subscript aero implies that only aerodynamic contributions are considered in C_T, C_L, and C_M. For this application, this detail is meaningless because inertial terms due to flapping or lagging blades are absent. The author has reported it for completeness.) This explicit formulation is derived from the most famous implicit one, nondimensional, written in a general coordinate system, which is worth quoting:

$$[M]\begin{bmatrix}\dot\lambda_0\\ \dot\lambda_s\\ \dot\lambda_c\end{bmatrix} + [L]^{-1}_{\text{nl}}\begin{bmatrix}\lambda_0\\ \lambda_s\\ \lambda_c\end{bmatrix} = \begin{bmatrix}C_T\\ -C_L\\ -C_M\end{bmatrix}_{\text{aero}} \tag{4}$$

The transformation between the two formulations is well explained by the same author of the theory in a technical note[9] in which some aspects of the model are reviewed and corrected for practical applications. Essentially, it is the model rewritten in a more usable form, namely, a projection from a generic reference frame to a body reference frame. For further details the reader is invited to look over the work by Peters and HaQuang.[9] The general formulation, however, is useful because it gives a greater insight into how this theory can be applied widely. The $[M]$ matrix, for example, is nothing more that an inertia term that allows the effects of the time delay to be included in the buildup or decay of the inflow field. It is called apparent mass matrix; the problem of its evaluation has been the subject of extensive studies, first by Carpenter and Fridovich,[10] who introduced the intuitive concept of the rotor seen as an impermeable disk that, under the actions of instantaneous acceleration and rotation in still air, produces reactions forces. They suggested that the transient inflow through the rotor, in axial flight, could be taken into account by including an accelerating mass of air occupying 63.7% of the air mass of the circumscribed sphere of the rotor:

$$m_S = \tfrac{4}{3}\pi\rho R^3, \qquad m_A = \tfrac{8}{3}\rho R^3 \cong 0.637 m_S$$

$$m_{11} = m_A/\pi\rho R^3 = 8/3\pi \tag{5}$$

A similar concept was applied to the apparent inertia, which was estimated to be a certain percentage of the rotary inertia of the same sphere. Therefore, we have

$$[M] = \begin{bmatrix}8/3\pi & 0 & 0\\ 0 & 16/45\pi & 0\\ 0 & 0 & 16/45\pi\end{bmatrix} \tag{6}$$

What seems to be a fanciful idea was confirmed both by experimental tests and by the analytical study by Pitt and Peters.[11] This latter is quite interesting and leads us to the focus point: The development of this model is based on an extension of the actuator-disk theory and this means that no geometric parameters are involved in determining the matrix coefficients. It does not matter how many blades the rotor has, or what shape they are. Moreover, in adoption of the first-harmonic form of the model, as done here, even the pressure distribution has little influence on the matrix coefficients.

Similar deductions are valid also in the case of the $[L]_{\text{nl}}$ matrix. It is the function of the wake angle α (measured with respect to the rotor disk) and of the mass-flow parameter matrix $[V]$ that weighs the mass flow in relation to the associated action:

$$[L]_{\text{nl}} = [L][V]^{-1} \tag{7}$$

$$[L] = \begin{bmatrix}\frac{1}{2} & 0 & -\frac{15\pi}{64}\sqrt{\frac{1-\sin\alpha}{1+\sin\alpha}}\\ 0 & \frac{4}{1+\sin\alpha} & 0\\ \frac{15\pi}{64}\sqrt{\frac{1-\sin\alpha}{1+\sin\alpha}} & 0 & \frac{4\sin\alpha}{1+\sin\alpha}\end{bmatrix} \tag{8}$$

$$[V] = \begin{bmatrix}V_T & 0 & 0\\ 0 & V & 0\\ 0 & 0 & V\end{bmatrix} \tag{9}$$

This apparent digression is the basis for the remarks that, in some manner, justify the application of a model, developed for helicopter

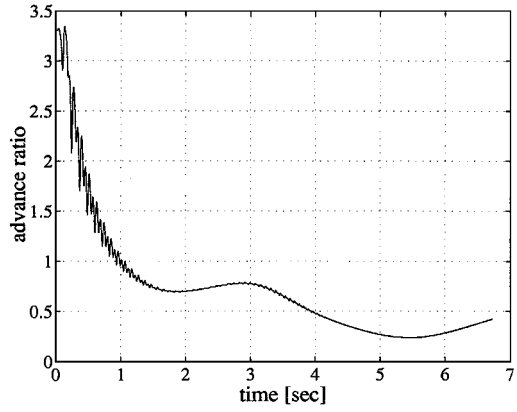

Fig. 6 Values of the advance ratio $\mu = \sqrt{(u^2 + v^2)}/rR$ during a complete flight.

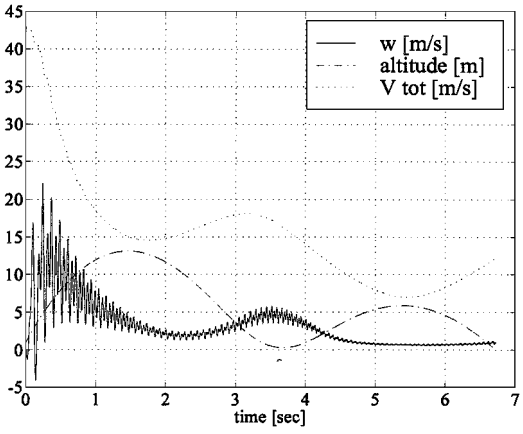

Fig. 7 Effect of altitude on the amplitude modulation (TA = 6.725 s).

rotors, to a very particular rotor, that is, an eccentric one. We conclude by observing that boomerang flight is performed at very high values of the advance ratio (see Fig. 6), when the induced velocities are nearly negligible with respect to the inflow due to forward motion. Nonetheless, their variations with time (unsteady effects) are consistent and this dynamic inflow model has been demonstrated to be a good evaluation tool, as is shown later.

The aerodynamic actions have been evaluated by using the blade-element theory: Forces and moments are calculated by the superposition of the contributions of each blade section, which is supposed to have the same characteristics as its constituting airfoil. Each elementary action has been evaluated by knowing the velocity components of the air relative to each point—thus the local angle of attack—and by interpolating the data extracted from the known airfoil characteristic curves. The elementary actions then were integrated numerically along the blade: This procedure is repeated each time the state vector derivative is calculated, i.e., four times per step, if an RK4 integration routine is used. This method is computationally expensive but conditions very far from linear may occur, especially where the blade is retreating and thus where wind blows from the trailing edge. At very high advance-ratio values, this reverse-flow region may be wide and a reliable evaluation of the aerodynamic actions might be impossible using the analytical integration (i.e., by assuming a constant lift slope and so on). A wind-turbine airfoil was chosen, the Wortmann FX84-W-127, whose characteristics were evaluated experimentally some years ago.[12] It demonstrated to be very suitable for this application because of its good autorotative qualities, which are required for the boomerang as well as for the wind-turbine airfoil. Figure 2 shows how rotational speed increases considerably, a symptom of the boomerang being only slightly slowed during its rotation; this allows for a very slow final descent, as shown in Fig. 7.

The mathematical system comprises 13 state equations (because the state vector $\boldsymbol{X}^T = [\boldsymbol{v}_B^T, \omega_B^T, \boldsymbol{q}^T, \boldsymbol{p}_{\text{NED}}^T]$ of the rigid body has 13 components) and 3 inflow equations [see Eq. (2)] which have been integrated in time with an RK4 routine. The sample time was chosen as a function of the rotational speed r: It was reduced until its further halving was demonstrated to be uninfluential on the results. Rotational speed r varies during the motion, and it may even double, so that in the simulation program an adaptative step option has been provided.

Analysis of a Flight

The mathematical system is nonlinear in 6 degrees of freedom, which results partly because of the particular motion of the boomerang. The time history and the stability of the system are strongly dependent on the throwing parameters and on the atmospheric conditions. To analyze the characteristic phases of a throw, let us refer to the solid curves of Fig. 8. They show the geographic trajectory, in terms of NED coordinates, performed by a test boomerang, the geometric parameters of which are reported in Table 1. In the next section, concerning the analysis of the influence of the parameters, this trajectory is always used as a term of comparison. Figures 2, 7, and 9 represent the same flight and can be useful in understanding the reasons for the boomerang's behavior. At the throw moment, the Euler angles are

$$\phi = -73.38 \text{ deg}, \qquad \theta = 52.62 \text{ deg}, \qquad \psi = 58.35 \text{ deg} \tag{10}$$

which means that the xy_B plane is nearly normal with respect to the ground and the xz_B plane has a small climbing ramp. In the first phase of the flight the system has a high translational speed, which, in the absence of wind, is the composition of the in-plane velocities u and v. The system takes off under the initial actions of great centrifugal and tangential accelerations, and, as soon as the aerodynamic forces become substantial, the trajectory bends and the w velocity component starts to develop. The boomerang begins its turn, and, as the translational speed decreases, the rotational speed

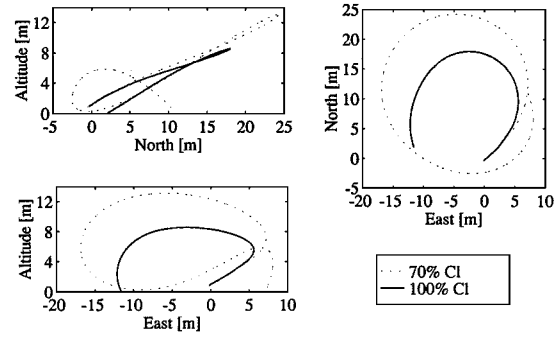

Fig. 8 Influence of aerodynamic characteristics (TA_1 = 2.445 s and $TA_{0.7}$ = 6.725 s).

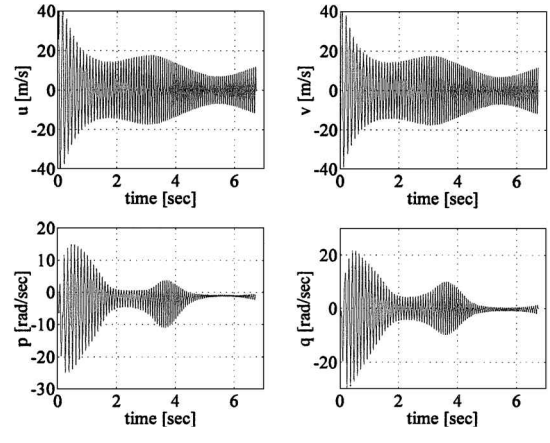

Fig. 9 Components of translational and rotational speed along the x_B and y_B axes (TA = 6.725 s).

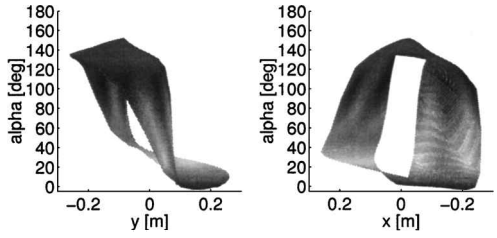

Fig. 10 Angles of attack of the advancing blade (time = 0.525 s).

can increase, decrease, or remain constant, depending on the autorotative characteristics of the system. Evidently, an increase in the rotational speed occurs at the cost of the translational one, for obvious energetic considerations. Thus, a highly autorotative boomerang covers small distances because it uses up a great amount of energy in whirring, but if the throw is performed with high power, the autorotative boomerang is able to complete its turn with a very slow descent, which is more spectacular as well as more precise. (This characteristic is associated with a certain form of stability, but this concept is more intuitive than mathematical.)

By analyzing the surfaces that represent the angles of attack, relative to a situation some instants after the throw (Fig. 10), we see that the blade is strongly loaded when its anomaly is some degrees greater than the reference position $\psi_a = 90$ deg (positive y_B axis). Lifting forces are concentrated there, and to a much greater extent, if we think that the advancing blade also has higher effective local velocities:

$$V_{\text{eff}} = \sqrt{U_P^2 + U_T^2} \tag{11}$$

where U_P is the parallel component of the local velocity with respect to the rotor disk, and U_T is the tangential one that strongly feels the effects of the forward speed. All of this means that, on average, this direction provides the position of the pressure center and subsequently of the precessing axis. In fact, the latter is defined as the intersection between the rotational plane and the plane that contains the couple, created by the lifting actions applied in the pressure center and the inertial and gravitational forces applied in the center of the mass. The precessing angular velocity vector, which lies on this axis, thus has both a component along the y axis and one along the x axis, and so, whereas the former is responsible for the further bending of the trajectory, the latter produces the flattening of the boomerang. The xy_B plane reduces its inclination with respect to the ground, slowly assuming a horizontal orientation, but this motion is quite unnoticable and the trajectory has time to complete itself before the flattening can take place. In the meantime, the body has reached its highest point, in correspondence to which the translational speed has a local minimum. The following glide occurs under the action of the gravitational field: The boomerang descends in autorotation with a strong recovery of kinetic energy; the translational and the rotational speeds increase while the rotational plane becomes more and more horizontal. This is the reason why, at a given instant, just at the end of the flight when the body is landing, the trajectory turns to climb, because the lifting actions have assumed the z_{NED} direction. The trajectory now has accomplished a complete turn and, depending on the amount of residual power and, more significantly, on the presence of wind, it can end in a number of different ways: If the airfoils that make up the boomerang have a high efficiency value, the trajectory goes on to another turn, as long as there is sufficient power; it may happen that, just before the end of the turn, the rotational plane tilts to the other side and the boomerang enters an opposite narrow turn, completing what is called the "eight." In the best case, the trajectory ends in a vertical autorotation in correspondence to the geographic initial point. What determines one situation instead of another? Figure 8 shows the comparison between two trajectories obtained under the same initial and environmental conditions, but in one case the airfoil efficiency was decreased by 30% with respect to the nominal efficiency. More precisely, the values of the drag coefficient have been kept constant, as have the moment coefficient ones, while the c_l curve has undergone a contraction equivalent to 30%. (This method also has practical applications: The boomerang is calibrated by the airfoil shape modifications to perform the desired trajectory. This means that the boomerang design does not require the high-efficiency condition at all costs.) The trajectory then becomes wider and reaches higher altitudes. In the case in which airfoils efficiency is unsatisfactory, the boomerang will not be able to perform its turn. In this case, experience teaches us that a slight positive tip incidence may be useful, but it also may compromise the boomerang's autorotative qualities.

Unsteady Effects and Parameter Influence on the Trajectory

Analysis of the parameters that influence the boomerang trajectory is accomplished numerically: The parameters are modified one at a time and the resulting trajectory is compared with a reference one. The parameters that are analyzed in this section concern environmental conditions, such as the wind direction, and throwing conditions, i.e., the power that the thrower puts into the boomerang and the inclination of the rotor-plane angle with respect to the ground. The influence of these parameters can be predicted easily because a skillful thrower plays exactly on them to calibrate the throwing. Therefore, this analysis can be seen as a preliminary verification of the mathematical model.

Besides the aforementioned influence of the external parameters, the importance and the value of the unsteadiness hypothesis that surrounds the model are evaluated. The hypothesis to be verified is whether the modelization of the unsteady effects is actually necessary, or if a steady induced-velocity model can fit the problem. To answer this question, it is important to take a closer look at the boomerang's motion features. Figure 9 reports the trends of the in-plane linear and angular velocities u, v, p, and q, representative of the same flight. These variables show a behavior that, in one way, resembles a beat phenomenon, i.e., a sinusoid, whose frequency is imposed by the rotational speed r, modulated by a sinusoidal amplitude. This latter is strictly bound to the oscillations of the total translational speed, which, in turn, decreases and increases according to the trend of the boomerang to climb or to descend, but maintaining an average decreasing course. Figure 7 shows this; moreover, because the system is strongly nonlinear, the parameters of this damped beat oscillation will depend on the characteristics of the system as well as on the throwing conditions, which seem to be able to modify the system natural modes. In addition, note that the characteristic time associated with these oscillations is very short, meaning that the state variables change very quickly. (The term "characteristic time" is more suitable than the term "frequency," which generally denotes the presence of a periodic motion whose characteristic parameters can be univocally evaluated.) If this characteristic time were comparable to the time for the evolution of the aerodynamic actions, the steady aerodynamic model would lead to the same results as the unsteady one. Figure 11 reports a comparison between two trajectories, obtained with the same throw and environmental parameters, but in one case the unsteady effects have not been taken into account; that is, the induced velocity is the one that resolves the closed-loop problem,

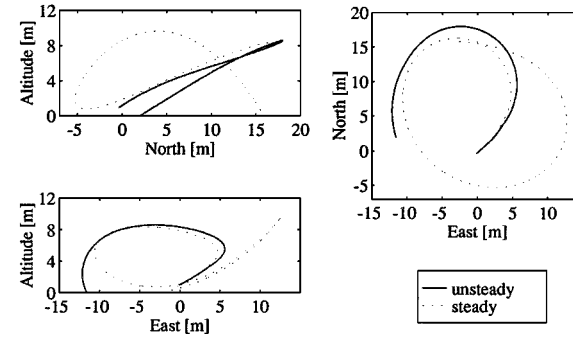

Fig. 11 Comparison between the steady and the unsteady model ($TA_{\text{st}} = 7.125$ s and $TA_{\text{unst}} = 2.445$ s).

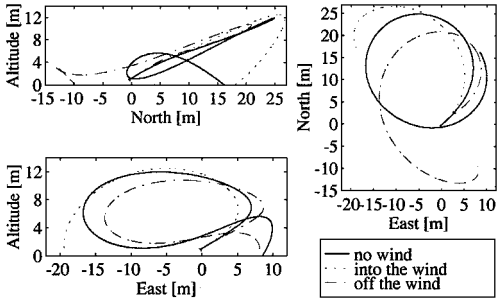

Fig. 12 Influence of the wind (TA_{into} = 3.025 s, TA_{off} = 6.225 s, and TA_{nw} = 6.735 s).

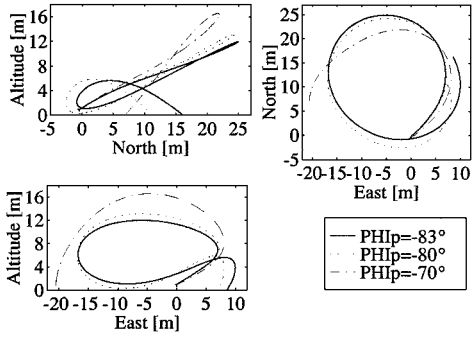

Fig. 13 Influence of the ϕ_P angle (TA_{70} = 3.350 s, TA_{80} = 6.725 s, and TA_{83} = 6.735 s).

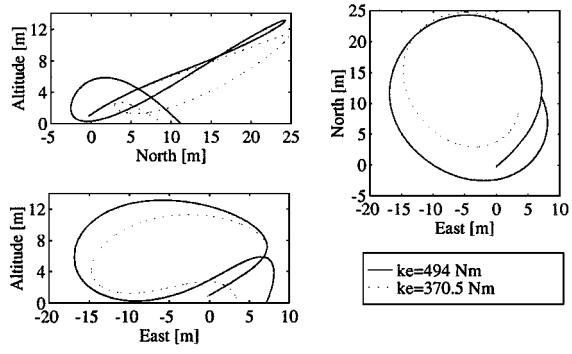

Fig. 14 Influence of the throwing power, as modified through the spring elastic constant k_e of the thrower machine (TA_{494} = 6.725 s and TA_{370} = 6.040 s).

which follows from Eq. (2) with $\dot{\lambda}_i = 0$. The differences are remarkable, especially in terms of time calculation. Resolving a closed-loop problem needs time of orders of magnitude greater than that required for the open-loop problem. The trajectory evaluated with the steady model clearly has something unnatural; indeed, it has never been verified with the real model. The boomerang seems to be pushed by very high aerodynamic forces, which, however, according to the unsteady model, do not have enough time to develop. This proves that the modelization of the unsteady effects is of utmost importance, because they actually affect the calculation of the boomerang's motion characteristics.

According to the conclusions that have just been drawn, the analysis of the parameters' influence will be carried out with the unsteady mathematical model.

Figure 12 shows the influence of the wind: A wind is blowing at 4 m/s northward (into the wind), and from the north (off the wind). A contrary wind subtracts a greater amount of energy from the system but the flight is longer; a favorable wind is less expensive in terms of energy, but the boomerang crashes to the ground in a few seconds. Throwers know this trend only too well, and so, the first rule learned is to throw about 45 deg off the wind.

Figure 13 shows another well-known behavior: In this case the varying parameter is the angle of inclination of the xy_B plane with respect to the xy_{NED} plane, at the throwing instant, i.e., the angle ϕ_P of inclination of the thrower-machine plane with respect to the ground. The more horizontal the angle, the higher the trajectory because the lifting force has a greater component along the z_{NED} direction. To run the additional 5 or 10 m of altitude, the body loses rotational kinetic energy; that is, the angular speed vector decreases and the precessing moments $\tilde{\omega}[J]\omega$ are no longer able to tilt the boomerang, and so, it crashes in a few seconds.

To conclude, Fig. 14 shows the influence of the throwing power: It is modified by varying the elastic constant k_e of the spring, which produces the bending moment on the thrower-machine arm. When a torsional spring is used, the bending moment is linear with k_e, so that a smaller value of k_e implies a lower throwing power. Apart from the last tract, the diameter of the trajectory appears unaffected, but the altitude is altered. This trend also has been detected and analyzed by other authors,[2,3] who agree in stating that the boomerang seems to "possess" its trajectory radius in itself.

Topographical Analysis of the Angle of Attack

Figures 10 and 15–17 are quite interesting. They show the topographical situation of the advancing blade angles of attack in four different phases of the motion, i.e., after about 0.5, 2.5, 4, and 5 s from the throwing instant. They were traced by mapping, instant by instant, the whole turn of the advancing blade. The central part, which is insignificant, is erased because it corresponds to a pressure hole. However, it is of no easy interpretation; in fact, this area would not be swept by the blades if the body did not have a forward motion. Where the angle of attack α is greater than 90 deg, it is possible to recognize the reverse-flow region. Initially, it is rather wide, but it narrows during the flight and this is perfectly coherent. In fact, the local angle of attack is due to the superposition of an increasing rotational speed r and a decreasing total translational one. At the end of the flight, the rotational speed is very high, so that it prevails over the translational one and the reverse-flow region disappears.

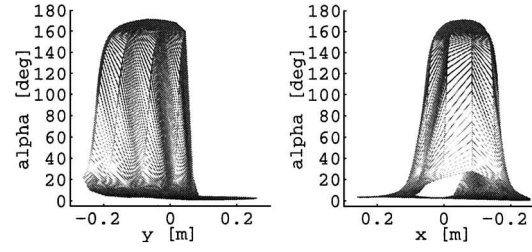

Fig. 15 Angles of attack of the advancing blade (time = 2.520 s).

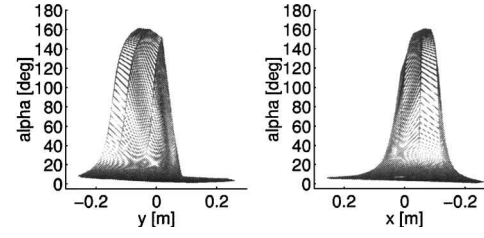

Fig. 16 Angles of attack of the advancing blade (time = 4.110 s).

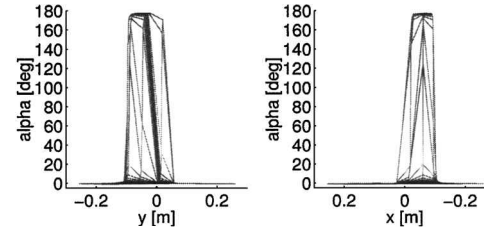

Fig. 17 Angles of attack of the advancing blade (time = 5.030 s).

Conclusions

The results presented show that this simulation program is able to deal with strongly unsteady motions, such as the boomerang flight. The boomerang is seen as a rotor working at a very high advance ratio; no geometric limitation is imposed, so that behavior of boomerangs of different shapes and dimensions can be compared. The influence of different environmental and throw parameters on a test boomerang are shown. Unsteady effects, which are predominant during the whole flight, are well dealt with by the Pitt–Peters[11] dynamic inflow model. Unlike other models, this latter model is based on the resolution of an open-loop program, so that a complete flight (which takes some seconds) can be simulated in a few minutes.

References

[1]Valenti, M., "The Return of the Boomerang," *Mechanical Engineering*, Vol. 115, No. 12, 1993, pp. 68–70.

[2]Hess, F., "L'Aerodinamica del Boomerang," *Scienze*, Vol. 2, No. 8, 1969, pp. 36–48.

[3]Pignone, G. A., *Boomerang: Fascino di Un'arma Preistorica*, Editoriale Olimpia, Firenze, Italy, 1986 pp. 9–106.

[4]Curtiss, H. C., and Shupe, N. K., "A Stability and Control Theory for Hingeless Rotor," *Proceedings of the 27th Annual National Forum of the American Helicopter Society*, Washington, DC, May 1971.

[5]Sissingh, G. J., "The Effect of Induced Velocity Variation on Helicopter Rotor Damping Pitch and Roll," Aeronautical Research Council, ARCTR–GP 101, England, UK, 1952.

[6]Chen, R. T. N., "A Survey of Nonuniform Inflow Models for Rotorcraft Flight Dynamics and Control Applications," *Vertica*, Vol. 14, No. 2, 1990, pp. 147–184.

[7]Gaonkar, G. H., and Peters, D. A., "Review of Dynamic Inflow Modeling for Rotorcraft Flight Dynamics," *Vertica*, Vol. 12, No. 3, 1988, pp. 213–242.

[8]Wagner, H., "Über die Entstehung des Dynamischen Auftriebes von Tragflügeln," *ZAMM*, Vol. 5, No. 1, 1925, pp. 17–35.

[9]Peters, D. A., and HaQuang, N., "Dynamic Inflow for Practical Applications," *Journal of the American Helicopter Society*, Vol. 33, No. 4, 1988, pp. 64–68.

[10]Carpenter, P. J., and Fridovich, B., "Effect of a Rapid Blade Pitch Increase on the Thrust and Induced Velocity Response of a Full Scale Helicopter Rotor," NACA TN 3044, 1953.

[11]Pitt, D. M., and Peters, D. A., "Theoretical Prediction of Dynamic-Inflow Derivatives," *Vertica*, Vol. 5, No. 1, 1981, pp. 21–34.

[12]D'Angelo, S., and Gili, P. A., "Wind Tunnel Measurements of Aerodynamic Coefficients of Asymmetrical Airfoil Sections for Wind Turbine Blades Extended to High Angle of Attack," Wind Energy-2, *Proceedings of the Second Contractors' Meeting*, Harwood Academic Pub., Amsterdam, Nov. 1987, pp. 297–308.